

# We are IntechOpen, the world's leading publisher of Open Access books Built by scientists, for scientists

5,800

Open access books available

142,000

International authors and editors

180M

Downloads

Our authors are among the

154

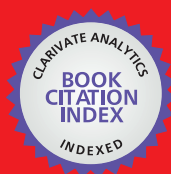
Countries delivered to

TOP 1%

most cited scientists

12.2%

Contributors from top 500 universities



WEB OF SCIENCE™

Selection of our books indexed in the Book Citation Index  
in Web of Science™ Core Collection (BKCI)

Interested in publishing with us?  
Contact [book.department@intechopen.com](mailto:book.department@intechopen.com)

Numbers displayed above are based on latest data collected.  
For more information visit [www.intechopen.com](http://www.intechopen.com)



## Chapter

# Filter Designs Based on Defected Ground Structures

*Somdotta Roy Choudhury*

## Abstract

This chapter concentrates on the filter structures using Defected Ground Structures (DGS). Initially, this chapter discusses the limitations of Electromagnetic Band Gap (EBG) structures and the development of DGS structure from EBG structure. DGS is an area of increasing interest in EBG technology. Here the well-known dumbbell DGS structures' features and physics are also discussed. New investigations are presented on the choice of geometrical shapes for the DGS structure as an element for the proposed filters. All the proposed DGS structures used to implement different types of filters (lowpass, bandpass, and bandstop) are validated.

**Keywords:** microstrip filter, defected ground Structures, bandstop filter, split ring, resonators

## 1. Introduction

Electromagnetic band gaps (EBGs) are generally periodic structures that exhibit different bandgaps over specific frequency ranges that prohibit electromagnetic wave propagation [1]. Due to its frequency selective characteristics, EBG structures naturally find applications in microwave filters. The main limitation of EBG structures is their large overall sizes and complex structures, which are not easy to analyse, and in most cases, not feasible to fabricate [2]. Defected Ground Structure (DGS) can overcome large size problems, and the complexity of EBG structures can be overcome by Defected Ground Structure (DGS). DGS structures can produce band rejection in specific frequency bands, and hence, is also known as a kind of EBG structure [3]. A DGS is a non-periodic EBG structure. It is an etched structure in the metallic ground plane of a microstrip structure. D. Ahn et al. first introduced the dumbbell-shaped DGS structure [4]. A variety of geometry etched in the microstrip line ground plane has been implemented to serve as defected ground structure. These structures usually add an extra lumped inductance and capacitance to the microstrip line connected as a parallel resonant circuit in series with transmission lines at both ends. The main features of the DGS structures are as follows in [5–12].

### 1.1 Some attractive features of DGS structure

Photonic Band Gap (PBG) Structures or Electromagnetic Band Gap (EBG) Structures could be:

- Periodic or non-periodic,
- Symmetric or non-symmetric,
- Easy to be presented as an LC equivalent circuit, and
- Simple and compact size.

### **1.2 Electrical characteristics of DGS structure**

- Disturbs the shielding fields on the ground plane.
- Increases effective permittivity.
- Decrease phase velocity and provide slow-wave characteristics.
- Increase effective capacitance and inductance of the transmission line under which it is placed.
- Provides bandstop characteristics.

### **1.3 Advantages of using DGS circuits**

- The structure is very much simple.
- Wider and deeper stopband characteristics.
- Provide low insertion loss.
- Have extremely small element values.
- Applications of DGS Structures:
  - Planar resonator.
  - High characteristic impedance transmission lines.
  - Microwave circuits such as filters.

Performance improvement of Coupler, Divider/Combiner, Oscillator, Power amplifier and Antenna etc.

## **2. Different filters using DGS**

The filter is one the most important parts of microwave circuit systems, and researchers have proposed different types of filtering circuits using DGS structures in recent years.

## 2.1 Performance improvement of lowpass filter using hexagonal head dumbbell shaped DGS

The hexagonal head dumbbell-shaped DGS is shown in **Figure 1**. The microstrip line is placed on the top plane and the proposed DGS on the ground plane. The different slot gaps,  $g = 0.2$  mm, transverse slot length,  $a = 2$  mm,  $b = 3.8$  mm, a width of the 50 Ohm microstrip line,  $W = 1.92$  mm.

### 2.1.1 Simulated results of unit cell

The structure is simulated by IE3D [11, 13] simulation software, and the simulated result shows a one-pole Butterworth prototype response given in **Figure 2**. The cutoff frequency is obtained at 3.3 GHz, and the transmission zero frequency is obtained at 5.1 GHz with attenuation of 23.9 dB. The sharpness factor is 11.6 dB/GHz.

### 2.1.2 Utility of the hexagonal slot

The advantages of the proposed hexagonal head DGS structure are: (1) for the equal effective area, the hexagonal shape of the slot provides increased path length for the current around the slot as compared to the square-headed slot and (2) for the equal value of resonant frequency the hexagonal slot area is 4.3% more compact than the square slot.

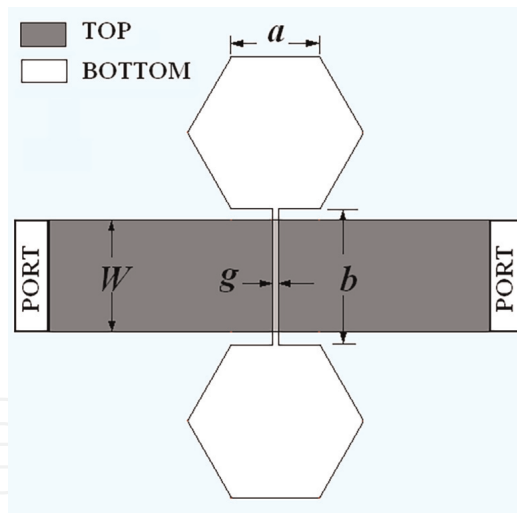


**Figure 1.**  
Schematic diagram of the hexagonal head dumbbell type DGS.

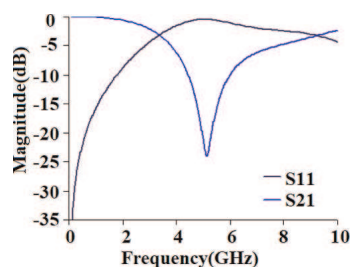


**Figure 2.**  
S-parameter response of DGS structure.

2.1.3 Parametric study of unit cell

Various parametric studies are performed to analyze the proposed DGS structure. Based on the hexagonal-head arm length, the inductance and capacitance of the filter are calculated and listed in **Table 1**. The S-parameter responses for different arm lengths “ $a$ ” of the hexagonal head are shown in **Figure 3**. The variation of the cutoff frequency (“ $f_c$ ”) and transmission zero frequency (“ $f_p$ ”) with respect to the arm length is plotted in **Figure 4**.

From **Table 1**, it is observed that the attenuation poles and attenuation zeros decrease with the increase of the arm length ( $a$ ) of the hexagonal head. With the increase of the arm length, the inductance value increases significantly, and the capacitance value remains almost constant. This is due to the increment in electrical path length around the hexagonal head slot. The change in inductance and capacitance values with different slot head lengths (“ $a$ ”) are given in **Figures 5 and 6**, respectively. Another parameter, transverse slot gap “ $g$ ,” also greatly affects the filter’s S-parameter response. The S-parameter responses for different transverse slots “ $g$ ” of the hexagonal dumbbell DGS are shown in **Figure 7**. The variation of the cutoff frequency ( $f_c$ ) and transmission zero frequency ( $f_p$ ) with respect to the transverse slot gap is plotted in **Figure 7**. With the increase of this slot, the gap capacitance changes, and correspondingly the current path along the hexagonal head also changes. As a result, the inductance of the structure also changes. This inductance and capacitance change with the structure dimension causes a change in the cutoff and pole frequency of the filter.

The change in the circuit elements are calculated and are tabulated in **Table 2**. It is clear from **Table 3** that the attenuation poles and attenuation zeros decrease with the increase of the transverse slot (“ $g$ ”) of the proposed DGS. With the increase of the transverse slot, the inductance value decreases minutely due to the small decrement

| Arm length of the Hexagonal Head ‘ $a$ ’ (mm) | 3 dB Cutoff frequency ‘ $f_c$ ’ (GHz) | Attenuation pole, ‘ $f_p$ ’ (GHz) | Capacitance ‘ $C$ ’ (pF) | Inductance ‘ $L$ ’ (nH) |
|---|---------------------------------------|-----------------------------------|--------------------------|-------------------------|
| 2   | 3.3                                   | 5.1                               | 0.202                    | 11.5                    |
| 4   | 2.5                                   | 4.1                               | 0.237                    | 17.0                    |
| 6   | 1.7                                   | 3.0                               | 0.301                    | 29.1                    |

**Table 1.** Circuit parameters of the Hexagonal Head Dumbbell DGS for different hexagonal head lengths “ $a$ .”

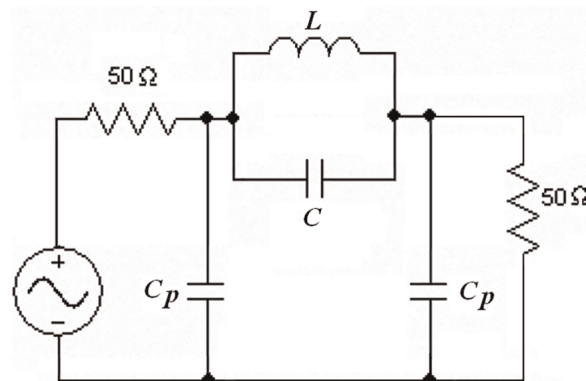


**Figure 3.** Equivalent circuit model of the hexagonal head dumbbell type DGS.

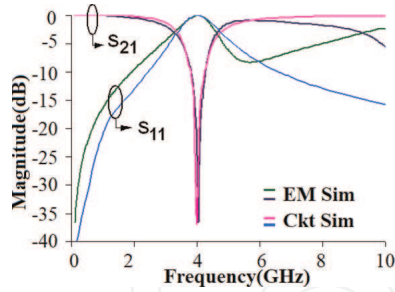


**Figure 4.**  
 Comparison of simulated and circuit model responses.

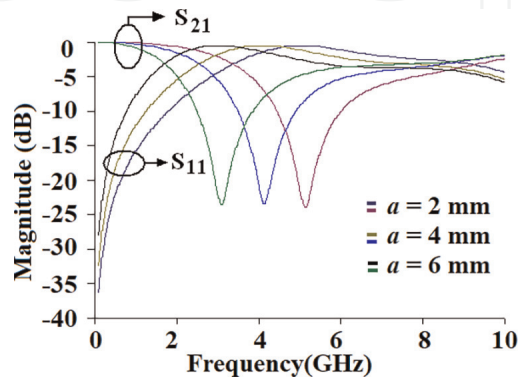


**Figure 5.**  
 Variations of simulated *s*-parameters with hexagonal head arm length “a.”

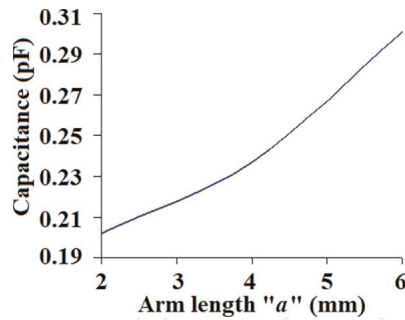


**Figure 6.**  
 Variations of equivalent capacitance with hexagonal head arm length “a.”

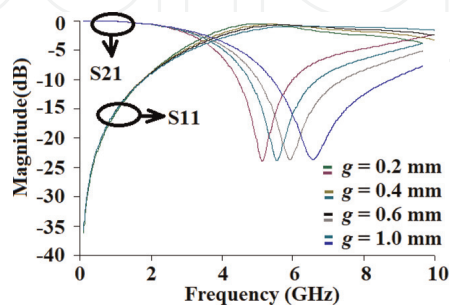


**Figure 7.**  
 Variation of simulated *S*-parameter responses with the change in the transverse slot gap “g.”

in the current path length. The capacitance value also decreases with the increase in the transverse slot. The inductance and capacitance values change with different slot gaps (“g”).

| Transverse slot gap 'g' (mm) | 3 dB Cutoff frequency 'f <sub>c</sub> ' (GHz) | Attenuation pole, 'f <sub>p</sub> ' (GHz) | Capacitance 'C' (pF) | Inductance 'L' |
|------------------------------|---|---|----------------------|----------------|
| 0.1                          | 1.76  | 3.7                                       | 0.26                 | 7.0            |
| 0.5                          | 1.79  | 4.2                                       | 0.19                 | 7.3            |
| 1.0                          | 1.83  | 4.7                                       | 0.16                 | 7.4            |
| 2.0                          | 1.87  | 5.3                                       | 0.12                 | 7.5            |

**Table 2.** Hexagonal Head Dumbbell DGS characteristics for different transverse slot gap “g.”

| No. of DGS unit | Pole frequency (GHz) | Cutoff Frequency (GHz) | Sharpness Factor (dB/GHz) | 20 dB Attenuation Band (GHz) |
|-----------------|----------------------|------------------------|---------------------------|------------------------------|
| Single          | 5.1                  | 3.3                    | 11.6                      | 0.36                         |
| Double          | 3.8                  | 3.1                    | 33.2                      | 2.10                         |
| Triple          | 2.8                  | 2.5                    | 84.3                      | 4.20                         |

**Table 3.** Comparative study among the filter structures using single, double, and-triple element hexagonal head dumbbell DGS.

#### 2.1.4 Improvement of the filter response by dual DGS units

The filtering response of the filter can be improved to higher-order by simply adding another hexagonal head DGS structure of the same dimension side by side with the previous one. The single hexagonal DGS unit provides poor selectivity (11.6 dB/GHz) and small 20 dB rejection bandwidth (360 MHz). Therefore to obtain a good transition between passband and stopband and broader stopband, an array of DGS structures can be used with high and low impedance microstrip lines [14]. The High-low line decreases the insertion loss and provides better matching in the input. Therefore, the main objective is to design an LPF implementing two hexagonal dumbbells DGS units. The schematic diagram of the filter is shown in **Figure 8**. The arm length of the hexagonal head dimension of the individual unit is  $a = 2$  mm with a separation of  $L = 2$  mm. The transverse slot dimension of each unit  $g = 0.2$  mm, etched out under the compensated transmission line of width,  $W_1 = 5$  mm. The transverse slot length,  $b = 3.8$  mm.

#### 2.1.5 Simulated response of double unit

The simulated S-parameter response is given in **Figure 9**. From the simulated S-parameter response, the array of two DGS units provides a lowpass filtering response with 3 dB cutoff frequency  $f_c = 3.1$  GHz, attenuation pole,  $f_p = 3.8$  GHz, and passband insertion loss of 0.5 dB. This also provides good transition (sharpness factor = 33.2 dB/GHz) between the passband and stopband and wider attenuation characteristics compared to single hexagonal head dumbbell DGS. The 20 dB rejection band is 2.1 GHz.

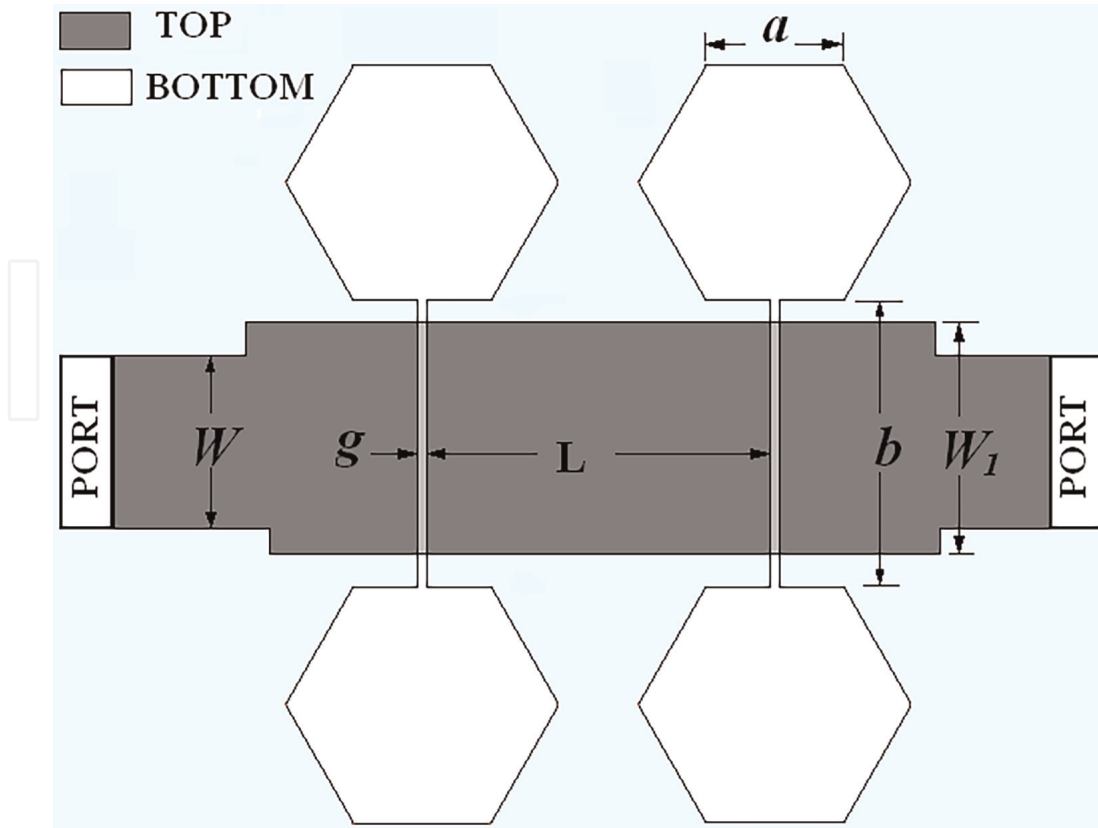


**Figure 8.**  
 Simulated S-parameter Response of two DGS units.

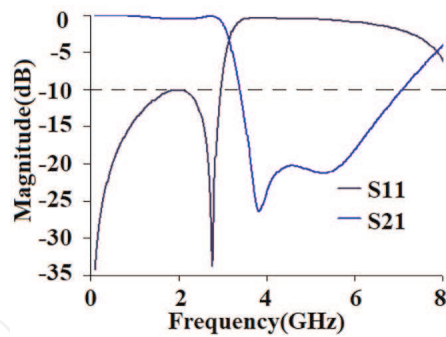


**Figure 9.**  
 Layout of the LPF using an array of three DGS units.

### 2.1.6 Improvement of the filter response by triple DGS units

The performance of the lowpass filter can be improved again by increasing the number of DGS units in the array. Here three DGS units are placed side by side in the ground plane under the high-low line, and all the DGS units have the same dimension. The dimensions of the filter structure are as follows:  $a = 2$  mm,  $b = 3.8$  mm,  $g = 0.2$  mm,  $W = 1.92$  mm,  $W_1 = 5.6$  mm,  $W_2 = 11.8$  mm,  $L = 2$  mm. The layout of the proposed filter using three DGS units is shown in **Figure 10**.

### 2.1.7 Simulated responses

The S-parameter plot of the proposed filter using three DGS units is shown in **Figure 11**. From the response of the scattering parameters, it is observed that the array



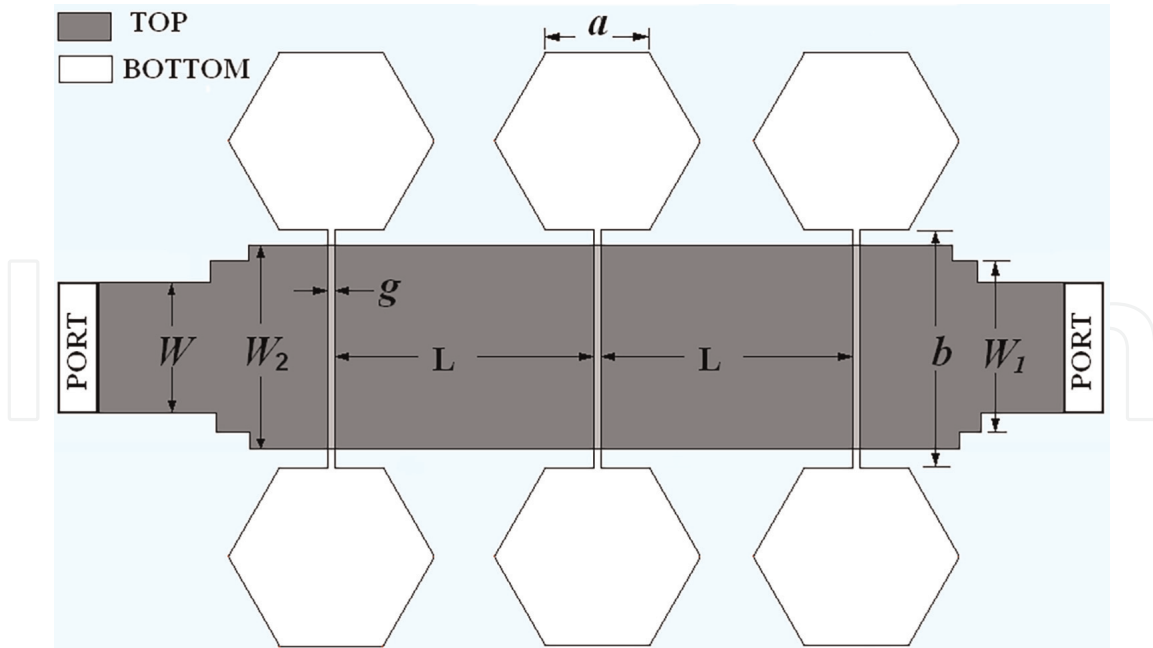


**Figure 10.**  
Layout of the LPF using an array of three DGS units.

of three DGS units provides a lowpass filtering response with 3 dB cutoff frequency,  $f_c = 2.5$  GHz, attenuation pole,  $f_p = 2.8$  GHz, and passband insertion loss of 0.6 dB. The sharpness of the passband edge of the filter is high, about 84.3 dB/GHz. The 20 dB rejection bandwidth is 4.2 GHz.

### 2.1.8 Measured results

The proposed structure is fabricated and measured by Vector Network Analyzer (VNA). The critical dimensions of the fabricated structure are  $a = 2$  mm,  $b = 3.8$  mm,  $g = 0.2$  mm,  $W = 1.92$  mm,  $W_1 = 5.6$  mm,  $W_2 = 11.8$  mm,  $L = 2$  mm. i.e., same as that of the simulation procedure. The photographic view of the structure is given in **Figure 12**. The comparison of the measured and simulated responses is shown in **Figure 13**.

The measurement result provides cutoff frequency = 2.6 GHz, Pole frequency = 3.06 GHz, insertion loss = 0.7 dB, 20 dB stop-band = 6.48 GHz, sharpness factor = 60.7 dB/GHz. The measured phase response is given in **Figure 14**. The discrepancy between measured and simulated phase responses is mainly due to the error resulting

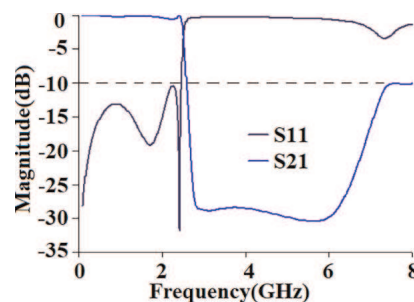


**Figure 11.**  
Simulated S- parameter Response of three DGS units.

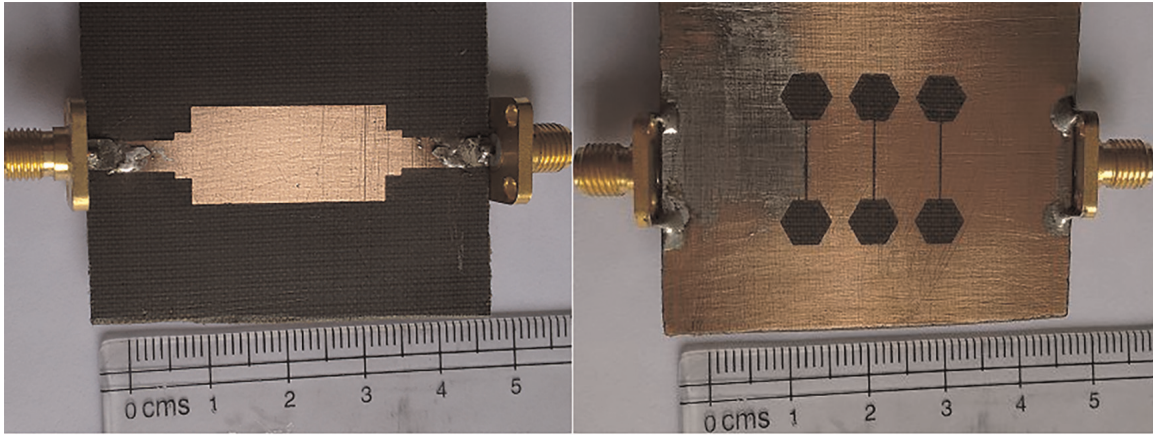


**Figure 12.**  
*Photographic view array of three DGS units.*

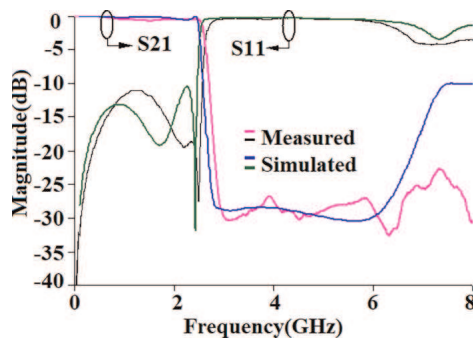


**Figure 13.**  
*Comparison of the Simulated and measured s-parameter responses of an array of three hexagonal-head DGS units.*

from manual calibration for measuring the phase. So it can be concluded that the present structure provides less insertion loss and better transition between passband and stopband compared to the array of two DGS structures. **Table 3** establishes a comparative study as given below. Thus, from this table, it is clear that the array with higher numbers of DGS units provides a more acceptable response than the array with lower numbers of DGS units. So it can be concluded that, although the big array of DGS units increases the circuit size and complexity, it delivers better filtering performance. **Figure 15** shows a graphical representation of the comparison of the transmission coefficients (S21) performances of the single, dual and triple unit hexagonal head DGSs. Thus, from this table, it is clear that the array with higher numbers of DGS units provides a more acceptable response than the array with lower numbers of DGS units. So it can be concluded that, although the big array

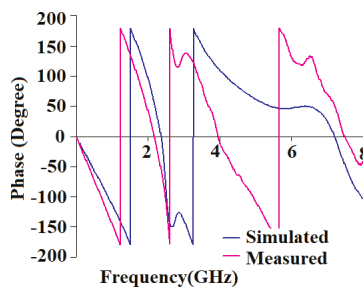


**Figure 14.**  
*Comparison of simulated and measured phase responses.*

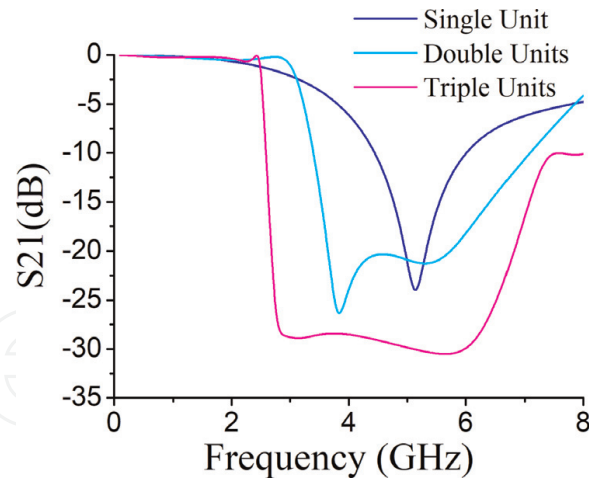


**Figure 15.**  
Comparison of the S-parameters of a single unit, double units, and triple units hexagonal DGSs.

of DGS units increases the circuit size and complexity, it delivers better filtering performance.

## 2.2 Bandstop filters using circular split-ring type defected ground structure

A compact bandstop filter using circular split-ring type DGS is designed. First, a unit cell circular ring type DGS with a split at the lower portion underneath a microstrip transmission line is analyzed. The microstrip line is placed on the top plane and the DGS on the ground plane, as illustrated in **Figure 16**. The different dimensions of the DGS unit are: - the outer radius of the ring,  $r_2 = 3.3$  mm, the inner radius of the ring,  $r_1 = 2.9$  mm, the width of the ring,  $g_1 = 0.4$  mm, the width of the gap,  $g_2 = 0.2$  mm, a width of the 50 Ohm microstrip line,  $W = 1.92$  mm.

### 2.2.1 Simulated result

The simulated response shows a one-pole bandstop type response. The attenuation zero frequency is obtained at 4.14 GHz, and attenuation pole frequency is obtained at

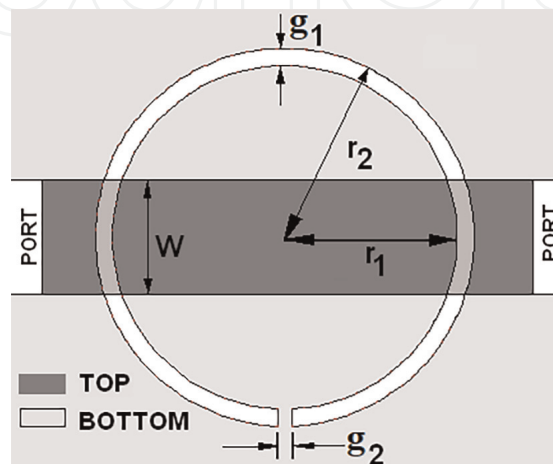


**Figure 16.**  
Schematic diagram of the circular split-ring type DGS.

4.5 GHz with attenuation of 31.5 dB, as shown in **Figure 17**. The sharpness factor at the lower passband edge is 79.17 dB/GHz. Maximum passband insertion loss is  $-0.07$  dB with a return loss greater than  $-18$  dB.

### 2.2.2 Parametric study

The stopband of the proposed bandstop filter can be tuned by simply changing the inner radius ( $r_1$ ), keeping the slot width ( $g_1$ ) and split gap ( $g_2$ ) of the ring DGS fixed, as shown in **Figure 18**. The ratios of cutoff frequencies and pole frequencies ( $f_c/f_0$ ) for different values of the ratios of inner radii and the 50-Ohm line width ( $r_1/W$ ) are plotted in **Figure 19**. The slot width ( $g_1$ ) of the split ring DGS also determines the cutoff and the pole frequency, keeping the outer radius ( $r_2$ ) and split gap ( $g_2$ ) at constant values as given in **Figure 20**. It is clear from **Figure 21** that changes in the ratios of the slot width to 50-ohm line width ( $g_1/W$ ) cause variation in the ratios of

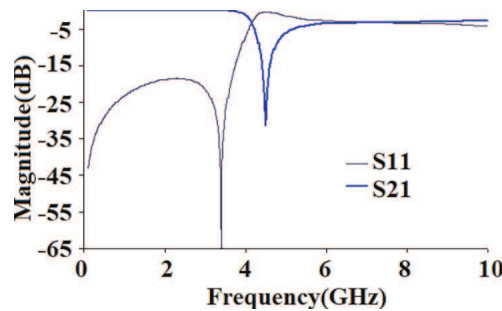


**Figure 17.**  
*S-parameters of the circular split-ring type DGS.*

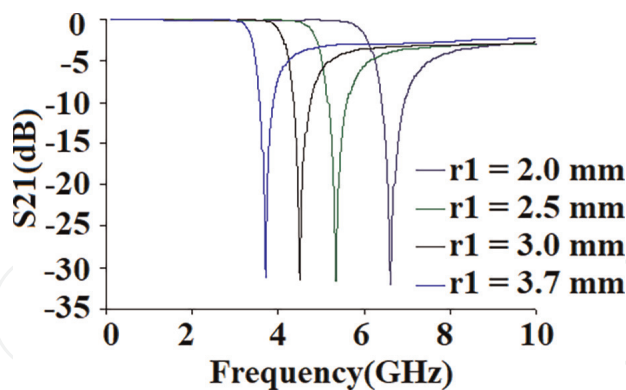


**Figure 18.**  
*Tuning of S-parameter responses with the inner radius ( $r_1$ ).*

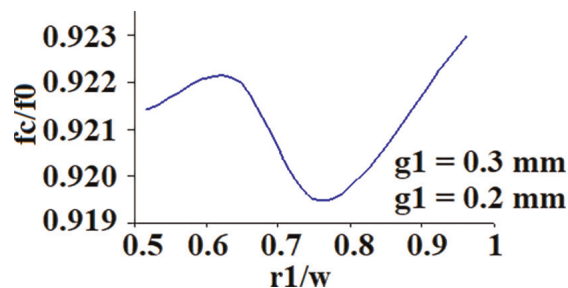


**Figure 19.**  
*Tuning of cutoff and pole Frequencies- with the slot width ( $g_1$ ).*

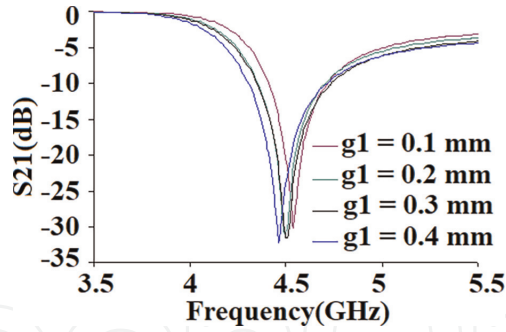


**Figure 20.**  
Tuning of S-parameter responses with the slot width ( $g_1$ ).

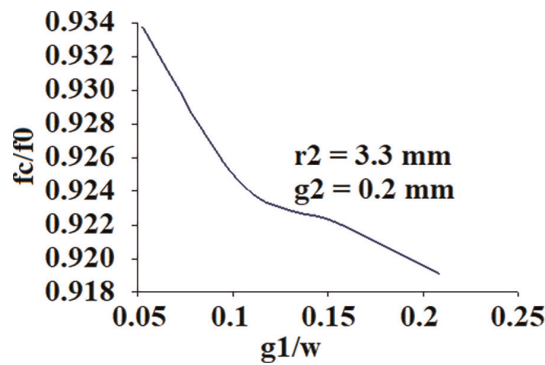


**Figure 21.**  
Variation of the ratios of cutoff and pole frequencies with slot width ( $g_1$ ).

cutoff frequencies and pole frequencies ( $f_c/f_0$ ). Again when studying the effect of the parameter  $g_2$  on the frequency response, it is obvious from **Figure 22** that  $g_2$  causes change in the values of cutoff and pole frequencies. The ratios of split gaps and the 50-ohm line widths ( $g_2/W$ ) are plotted with the ratios of cutoff frequencies and pole frequencies ( $f_c/f_0$ ), as shown in **Figure 23**.

### 2.2.3 Equivalent circuit parameters

Extracted equivalent-circuit parameters (equivalent inductance,  $L$  and capacitance,  $C$ ) of the proposed DGS unit section for different dimensions are calculated by (Eq. (1)) [4] and Eq. (2) [4] and listed in **Tables 4** and **5** given below.

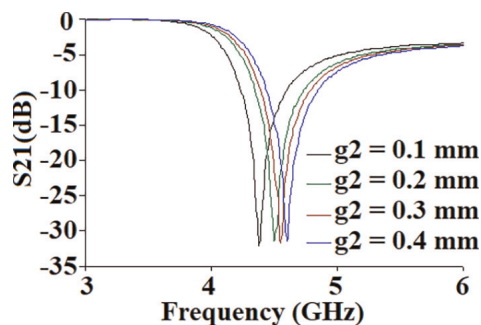


**Figure 22.**  
Tuning of S-parameter of  $f_c$  and  $f_0$  with a split gap ( $g_2$ ).

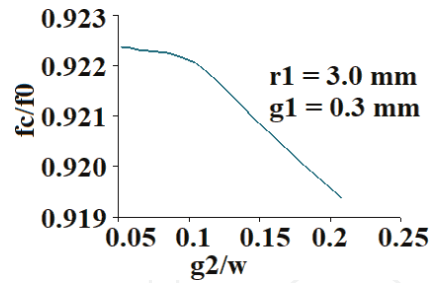


**Figure 23.**  
Variation of the ratios responses with the split gap ( $g_2$ ).

| Extracted Parameters & corresponding Frequencies | $r_1 = 2.0,$<br>$r_2 = 2.3$ (mm) | $r_1 = 2.5,$<br>$r_2 = 2.8$ (mm) | $r_1 = 3.0,$<br>$r_2 = 3.3$ (mm) | $r_1 = 3.7,$<br>$r_2 = 4.0$ (mm) |
|--|----------------------------------|----------------------------------|----------------------------------|----------------------------------|
| Inductance, $L$ (nH)                             | 0.19                             | 0.50                             | 0.57                             | 0.70                             |
| Capacitance, $C$ (pF)                            | 1.49                             | 1.77                             | 2.18                             | 2.63                             |
| Cutoff Frequency, $f_c$ (GHz)                    | 6.11                             | 4.91                             | 4.14                             | 3.40                             |
| Pole Frequency $f_0$ (GHz)                       | 6.62                             | 5.34                             | 4.49                             | 3.69                             |

**Table 4.**  
Extracted equivalent-circuit parameters of the proposed split ring DGS unit section having dimensions  $g_1$  and  $g_2$  kept fixed ( $g_1 = 0.3$  mm;  $g_2 = 0.2$  mm).

| Extracted Parameters & corresponding Frequencies | $r_1 = 3.2,$<br>$g_1 = 0.1$ (mm) | $r_1 = 3.1,$<br>$g_1 = 0.2$ (mm) | $r_1 = 3.0,$<br>$g_1 = 0.3$ (mm) | $r_1 = 2.9,$<br>$g_1 = 0.4$ (mm) |
|--|----------------------------------|----------------------------------|----------------------------------|----------------------------------|
| Inductance, $L$ (nH)                             | 0.48                             | 0.55                             | 0.57                             | 0.60                             |
| Capacitance, $C$ (pF)                            | 2.56                             | 2.24                             | 2.18                             | 2.11                             |
| Cutoff Frequency, $f_c$ (GHz)                    | 4.23                             | 4.16                             | 4.14                             | 4.09                             |
| Pole Frequency, $f_0$ (GHz)                      | 4.53                             | 4.50                             | 4.49                             | 4.45                             |

**Table 5.**  
Extracted equivalent-circuit parameters of the proposed split ring DGS unit section having dimensions  $r_2$  and  $g_2$  kept fixed ( $r_2 = 3.3$  mm;  $g_2 = 0.2$  mm).

$$C = \frac{\omega_c}{Z_0 g_1 (\omega_0^2 - \omega_c^2)} \quad (1)$$

$$L = \frac{1}{4\pi^2 f_0^2 C} \quad (2)$$

### 2.2.4 Improvement of the response

To increase the order of the bandstop filter, two split ring type DGS units are introduced in the ground plane under the 50-Ohm microstrip line, as shown in **Figure 24**. Here in this design, both the DGS units have equal dimensions. The dimensions of the DGS units are: - outer radii of the rings,  $r_2 = 3.3$  mm, inner radii of the rings,  $r_1 = 3.0$  mm, the widths of the rings,  $g_1 = 0.3$  mm, the widths of the gaps,  $g_2 = 0.2$  mm, the length between the two split ring units,  $L = 17.4$  mm, widths of the 50 Ohm microstrip line,  $W = 1.92$  mm.

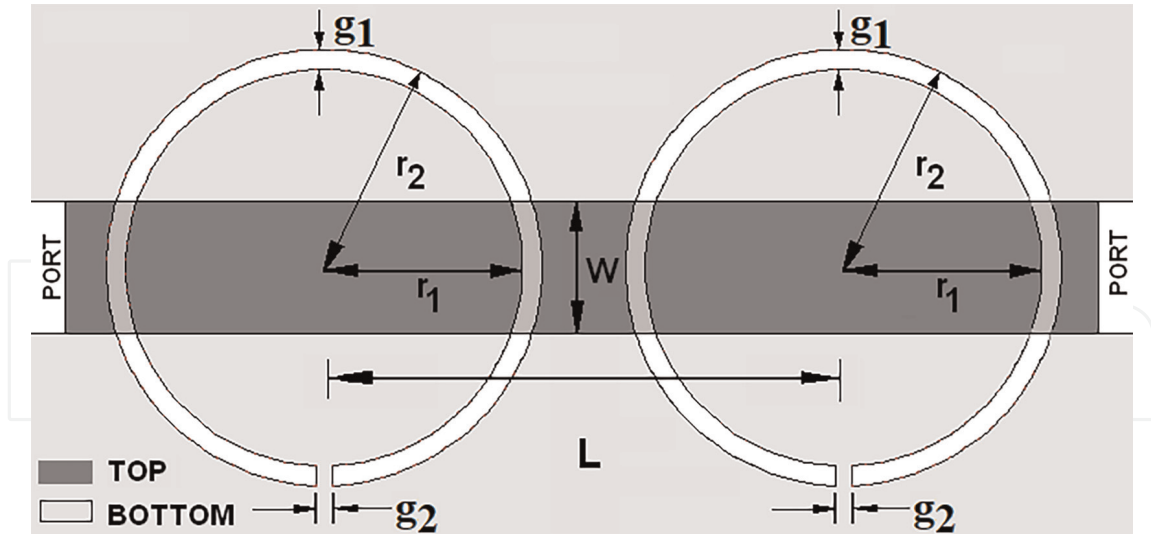


**Figure 24.**  
Schematic diagram of the lowpass filter using double unit split ring DGS.

### 2.2.5 Simulated result of dual units

The S-parameter response of this structure is given in **Figure 25**. It is clear from the figure that the filter has a cutoff frequency of 3.9 GHz and insertion loss of 0.1 dB. The sharpness of this filter is quite good, about 54 dB/GHz. The main disadvantage of the filter is the poor out-of-band performances, i.e., the stopband outside the passband only ranges from 4.38 GHz to 4.76 GHz at the attenuation level of -20 dB.

### 2.3 Improvement of out of band performance using open stub

This disadvantage can be overcome by introducing another transmission zero at the region of the stopband [15, 16]. An open circuited stub employed at the top plane creates this additional transmission zero, as shown in **Figure 26**. A compensated high-low impedance line is employed in the microstrip line above the DGS structure for matching purposes. The physical dimensions of the modified structure with open stub are:  $W_1 = 8.5$  mm,  $W = 1.92$  mm,  $g_1 = 0.3$  mm,  $g_2 = 0.2$  mm,  $L = 9.1$  mm,  $r_1 = 3$  mm,  $r_2 = 3.3$  mm. The shunt capacitor due to the stub is given by the following (Eq. (3)) [9].

$$\omega C_2 = \frac{1}{Z_{Oc}} \tan\left(\frac{2\pi W_1}{\lambda_g}\right) \quad (3)$$

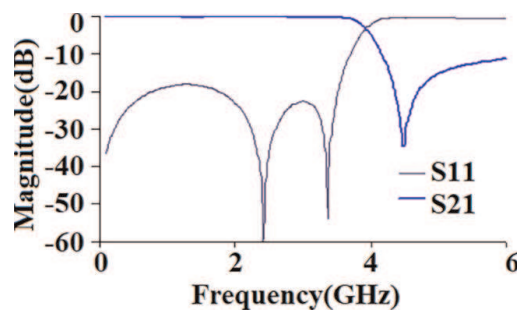


**Figure 25.**  
S-parameter result of the lowpass filter using double unit split ring DGS.

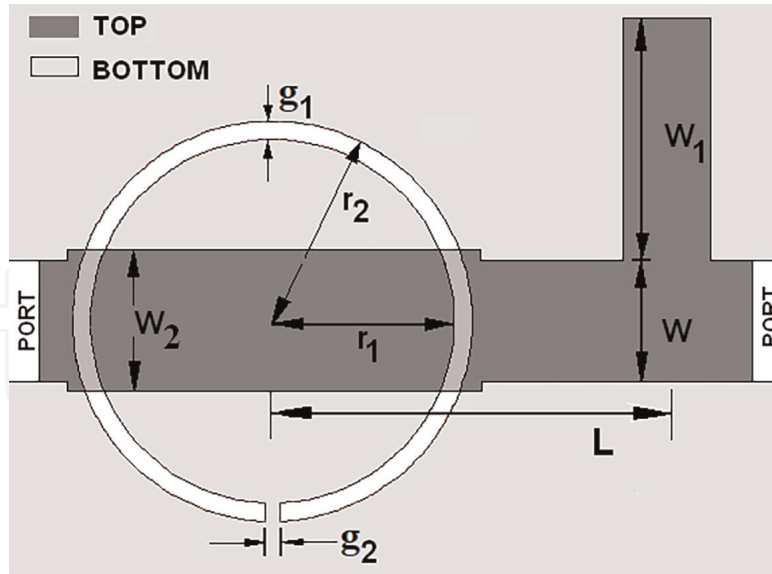


**Figure 26.**  
 Schematic diagram of the bandstop filter using a split ring DGS section and open-ended stub.

Here the left side of the equation is the susceptance of the shunt capacitor, and the right side of the equation represents the input susceptance of the open-circuited stub, which has the characteristic impedance “ $Z_{OC}$ ,” and the physical length “ $W_1$ ” ( $W_1 < \lambda_g/4$ ) of the stub. The physical length of the open circuted stub is determined by the (Eq. (4)) below [9].

$$W_1 = \frac{\lambda_{gc}}{2\pi} \tan^{-1} \omega_c C_2 Z_{OC} \quad (4)$$

### 2.3.1 Simulated response of the structure

The simulated S-parameter response is shown in **Figure 27**. Two prominent resonances are found in the response. The first one is at 4.7 GHz and is responsible for the DGS unit with the same dimensions as given above, and the second pole is at 5.1 GHz and is responsible for the stub. The upper and lower cutoff frequencies are 4.1 GHz and 5.9 GHz, respectively. The filter provides a  $-20$  dB bandwidth of 0.9 GHz and a rejection level of 30 dB. The sharpness of the lower and upper edge of the band are

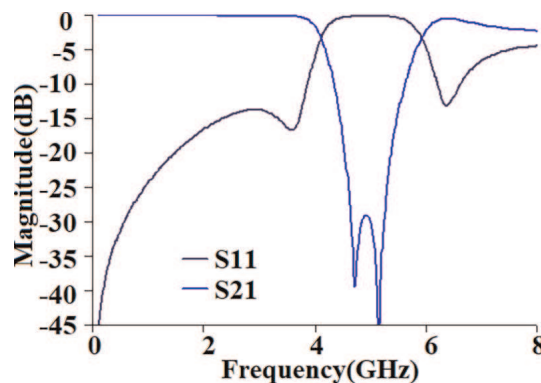


**Figure 27.**  
 S-parameter response of the lowpass filter using double unit split ring DGS sections and open-ended stub.



60.1 dB/GHz and 54.8 dB/GHz, respectively. Maximum insertion loss at the passband is 0.2 dB.

### 2.3.2 Equivalent circuit model of the filter

The equivalent circuit of the proposed filter is given in **Figure 28**, where circular split ring DGS is represented by a parallel resonant circuit connected in series with the source, and an open stub is referred to as a series resonant circuit connected in shunt with the source. The inductance ( $L_2$ ) is obtained due to the high value of  $Z_{0c}$ . The comparison of the simulated and circuit response is given in **Figure 29**.

### 2.3.3 Parametric study of the filter

By changing either the dimension (both inner radius “ $r_1$ ” and outer radius “ $r_2$ ”) of the split ring DGS or the dimension of the stub (stub length “ $W_1$ ”), the stopband of the filter can be controlled as shown in **Figures 30** and **31**. The changes of the ring radius and width of the stub with respect to the cutoff and pole frequency are clearly explained by **Figures 32** and **33**, respectively.

The corresponding mathematical expressions for the cutoff and pole frequency of the filter varying with inner radius “ $r_1$ ” and stub length “ $W_1$ ” can be obtained from the Eqs. (5)–(8).

$$f_{c1} = -0.72r_1^2 + 3.88r_1 - 0.86 \tag{5}$$

$$f_{p1} = -0.83r_1^2 + 4.35r_1 - 0.8 \tag{6}$$

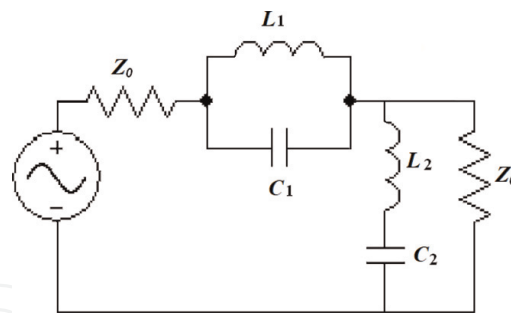


**Figure 28.**  
Equivalent circuit of proposed bandstop filter.

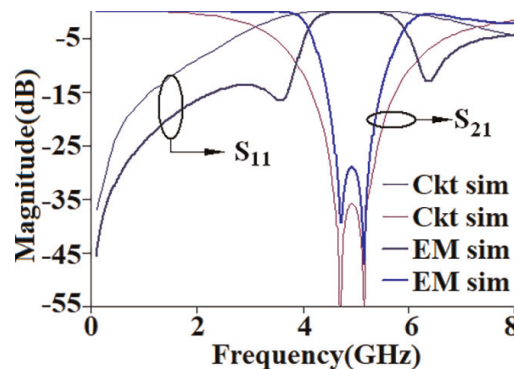


**Figure 29.**  
Comparison of the simulated and circuit response.

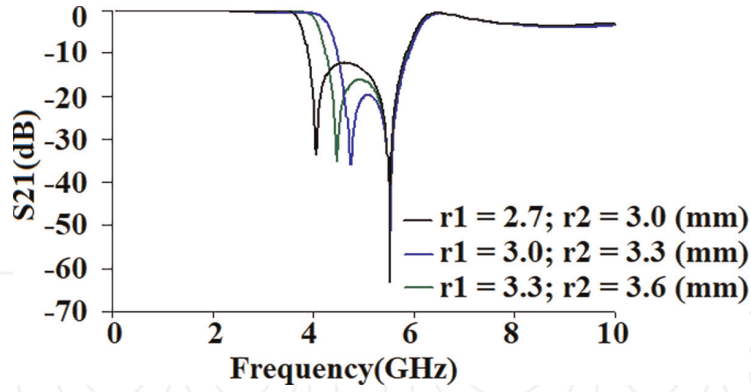


**Figure 30.**  
 Variation of S-parameters magnitudes w.r.t outer and inner radii ( $r_2, r_1$ ).

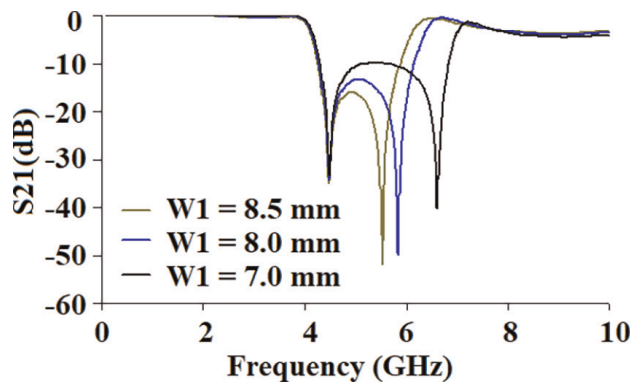


**Figure 31.**  
 Variation of the magnitude of S-parameters w.r.t length ( $W_1$ ) of the open-ended stub.

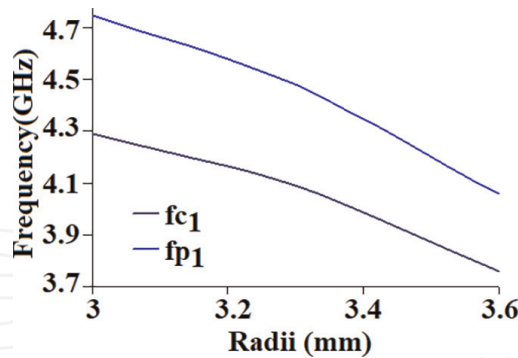


**Figure 32.**  
 Change of cutoff and pole frequencies with outer and inner radii ( $r_2, r_1$ ).

$$f_{c2} = -0.006W_1^2 + 0.07W_1 + 3.97 \quad (7)$$

$$f_{p2} = 0.08W_1^2 - 2.07W_1 + 16.86 \quad (8)$$

#### 2.3.4 Surface current distribution of the filter

**Figures 34 and 35** show the surface current distribution of the filter. At the first resonance, the magnetic current distribution in the split ring DGS is maximum, whereas the electric current density at the stub is negligible.

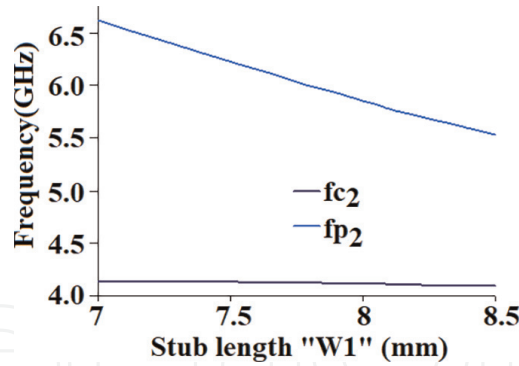


**Figure 33.** Change of cutoff and pole frequencies with length ( $W_1$ ) of the open-ended stub.

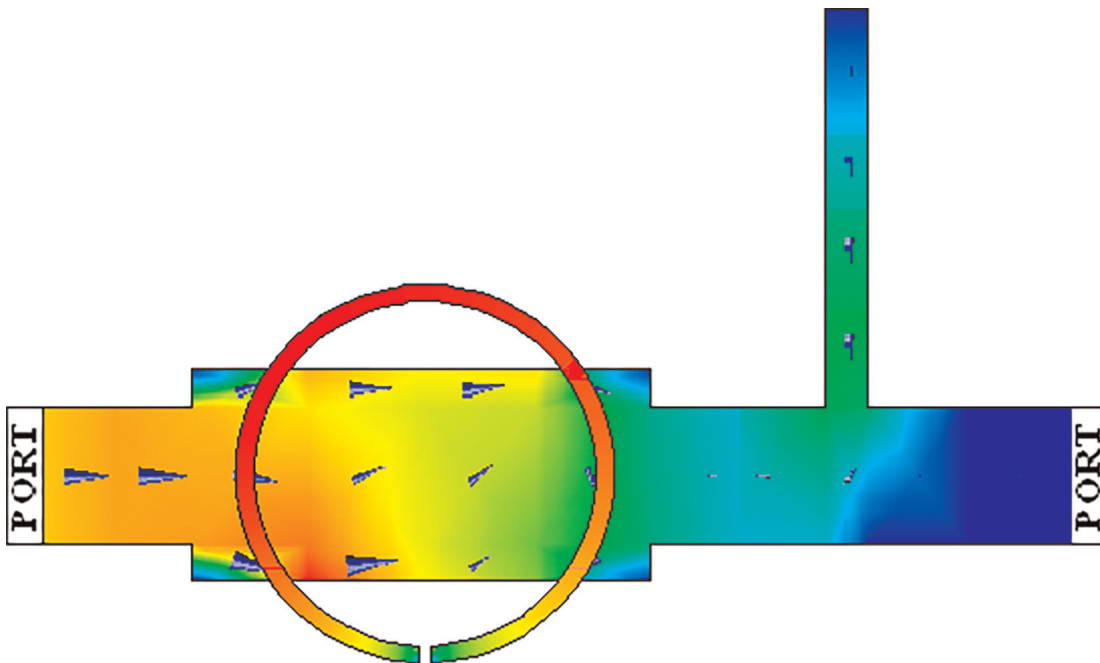


**Figure 34.** Surface electric and Magnetic current distribution at 4.71 GHz.

During the second resonance, the split ring DGS's magnetic current is minimal, and the surface electric current distribution is maximum through the stub. The conclusion for the phenomena can be explained, such as that the split ring DGS is responsible for the first resonance whereas the stub provides the second resonance.

### 2.3.5 Measured result

The prototype fabrication and measurement verify the proposed filter design using the Vector Network Analyzer (VNA). The photographic view of the structure for the top plane and ground plane is illustrated in **Figures 36** and **37**, respectively. It is found in **Figure 38** that simulation and measured S-parameter results are in good agreement. **Figure 39** shows the measured phase response almost linear in the passband region.

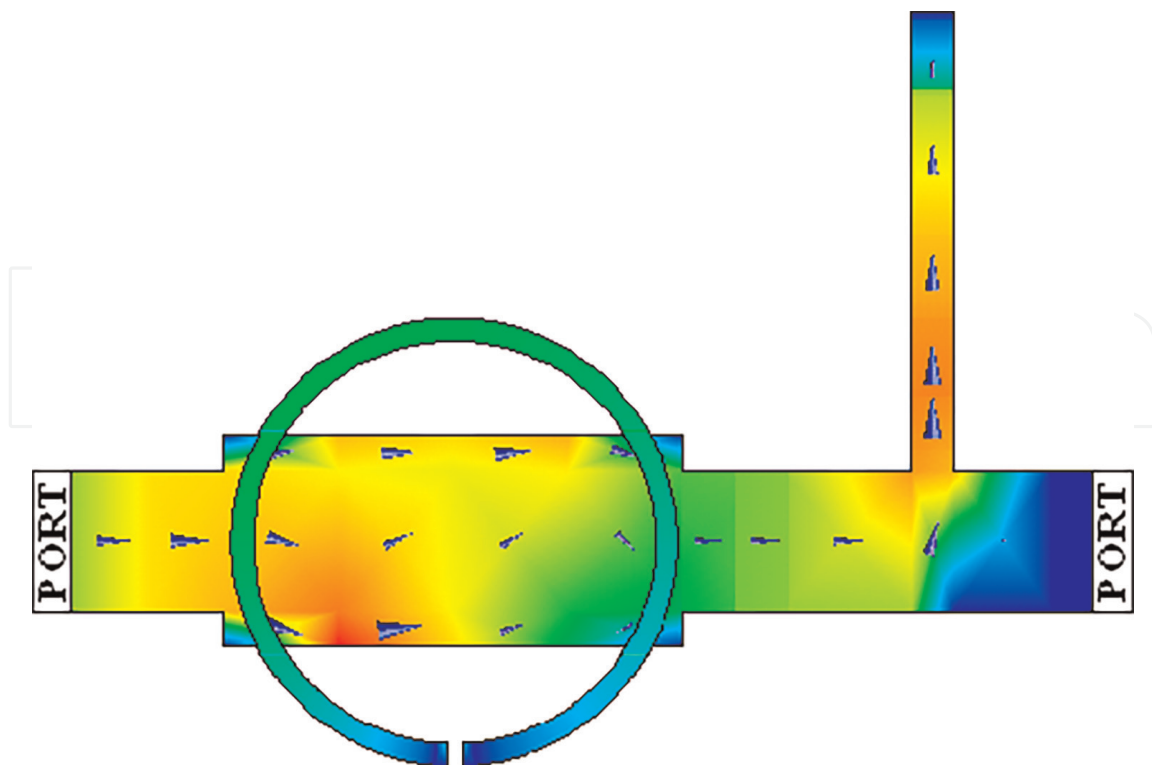


**Figure 35.**  
*Surface electric and Magnetic current distribution at 5.16 GHz.*

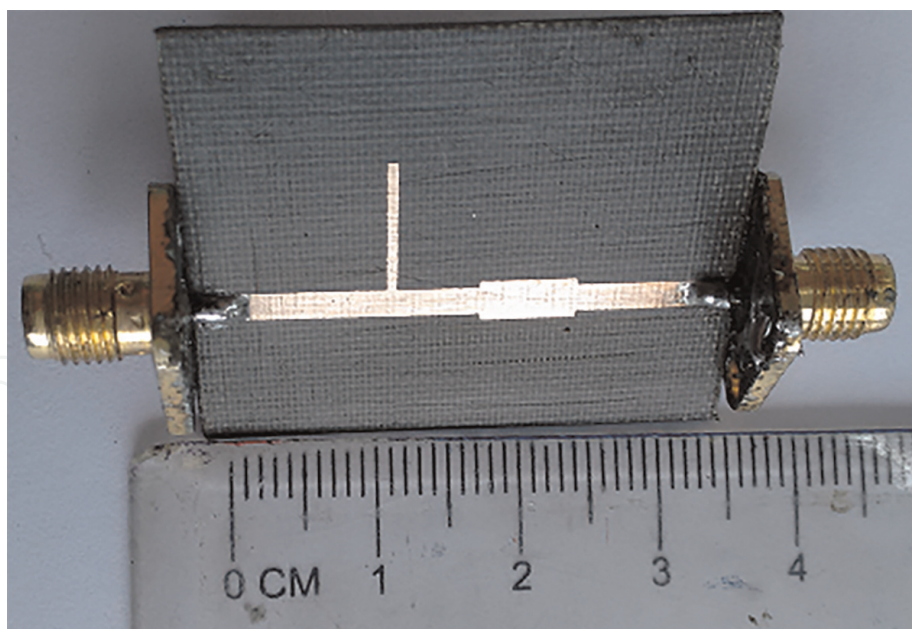


**Figure 36.**  
*Photographic view of the Top plane of the Split-ring DGS with Open-stub.*

#### **2.4 Increment of bandwidth and roll-off factor of lowpass filter by circular split ring DGS**

Another technique is proposed here to increase the stopband, which involves the combination of a third-order lowpass filter (LPF) with bandstop filters. The first step is to design a microstrip elliptic function lowpass filter to develop this filter. The

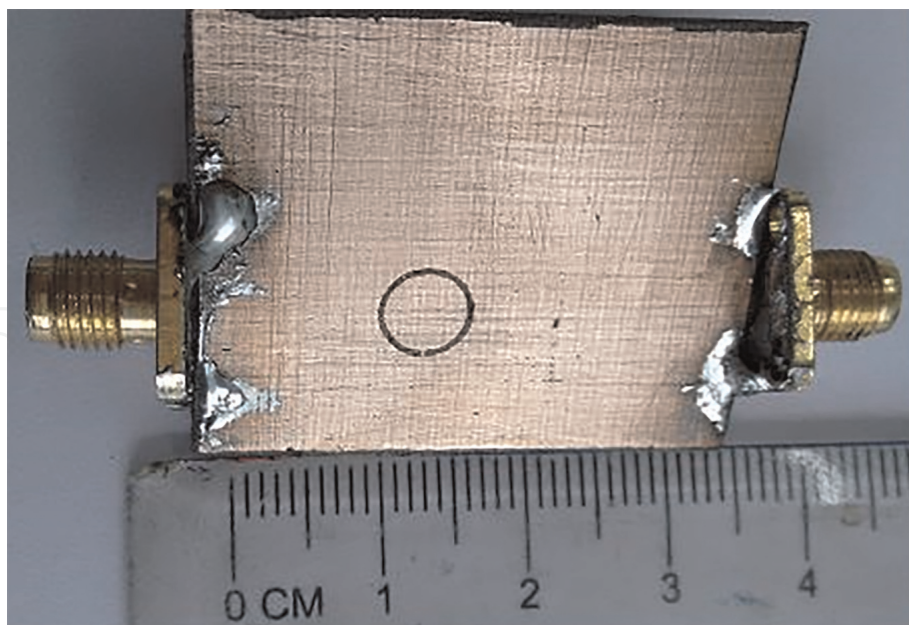


**Figure 37.**  
*Photographic view of the bottom plane of the Split-ring DGS with Open-stub.*

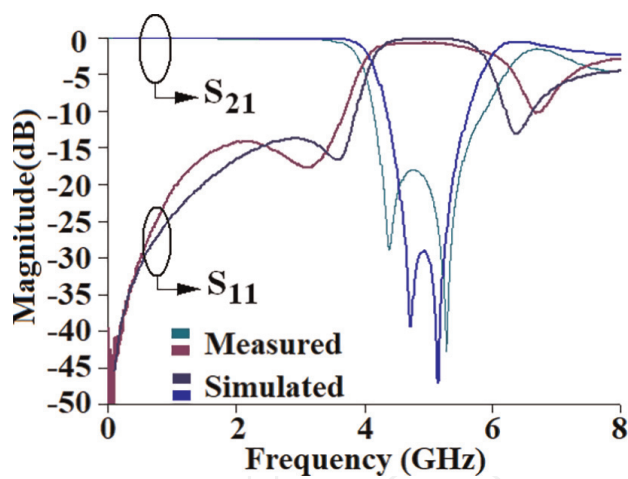


**Figure 38.**  
*Comparison of the simulated and measured s-parameter results.*

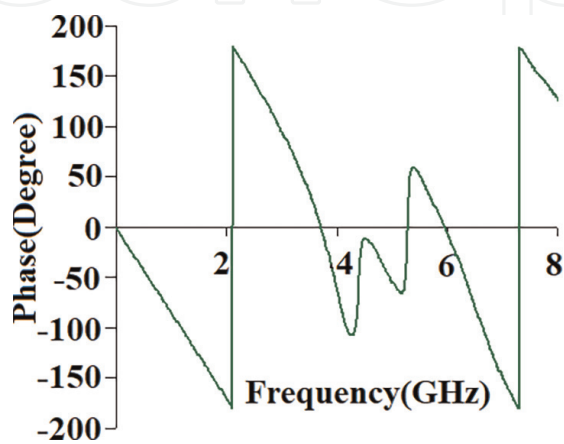


**Figure 39.**  
*Measured phase responses.*

elliptic filter is chosen due to its sharper cutoff rate for a given number of reactive elements [4]. The bandstop responses are obtained by split ring type DGS units of different sizes. The main purpose of these DGS units is to increase the bandwidth of the rejection band.

#### 2.4.1 Analysis of different LC elements and parameters

The L-C element values, scaled to  $Z_0$  and  $f_c$  are determined by the following equations (Eqs. (9) and (10)):

$$L_i = \frac{1}{2\pi f_c} Z_0 g_{Li} \quad (9)$$

$$C_i = \frac{1}{2\pi f_c} \frac{1}{Z_0} g_{Ci} \quad (10)$$

The element values of the third-order elliptic function lowpass prototype are given in **Table 6**, with corresponding L-C values derived from the above equations. All the inductors are realized using high impedance lines with characteristic impedance  $Z_{0L} = 93$  Ohms, whereas all the capacitances are realized using low impedance lines with characteristic impedance  $Z_{0C} = 14$  Ohms. **Table 7** lists all relevant microstrip design parameters calculated using the microstrip design equations [10]. Corresponding design parameters are substituted from **Tables 6** and **7** in the following equations (Eqs. (11) and (12)) to realize the initial physical lengths of the high and low impedance lines and are listed in **Table 8**. The layout of this third-order elliptic function LPF with the design dimension is given in **Figure 40**.

| g <sub>0</sub> = g <sub>4</sub> = 1.0, Normalized cut off, Ω <sub>c</sub> = 1, Passband Ripple, L <sub>Ar</sub> = 0.1 dB. |   |   |   |   |
|---|---|---|---|---|
| Element Values for Elliptic Function LPF prototype  | g <sub>L1</sub> = g <sub>1</sub> = 0.8214 | g <sub>L2</sub> = g <sub>2</sub> = 0.3892 | g <sub>C2</sub> = g <sub>2</sub> = 1.0840 | g <sub>L3</sub> = g <sub>3</sub> = 1.1880 |
| L-C element values  | L <sub>1</sub> = 1.64 nH                  | L <sub>2</sub> = 0.77 nH                  | C <sub>2</sub> = 0.86 pF                  | L <sub>3</sub> = 2.36 nH                  |

**Table 6.** LPF prototype elements values and L-C element values for third-order elliptic function LPF.

|  |                         |                         |                         |
|--|-------------------------|-------------------------|-------------------------|
| Characteristic impedance (ohms)          | Z <sub>0c</sub> = 14    | Z <sub>0</sub> = 50     | Z <sub>0L</sub> = 93    |
| Microstrip line width (mm)               | W <sub>C</sub> = 10.03  | W <sub>0</sub> = 1.92   | W <sub>L</sub> = 0.59   |
| Guided wavelength at f <sub>c</sub> (mm) | λ <sub>gC</sub> = 44.12 | λ <sub>g0</sub> = 46.97 | λ <sub>gL</sub> = 48.72 |

**Table 7.** Microstrip design parameters for the elliptic function LPF with a dielectric constant of the substrate 3.2 and substrate height = 0.79 mm.

|                      |                      |                      |                      |
|----------------------|----------------------|----------------------|----------------------|
| l <sub>L1</sub> (mm) | l <sub>L2</sub> (mm) | l <sub>C2</sub> (mm) | l <sub>L3</sub> (mm) |
| 3.56                 | 1.63                 | 2.16                 | 5.37                 |

**Table 8.** Initial physical lengths of the corresponding L-C parameters.

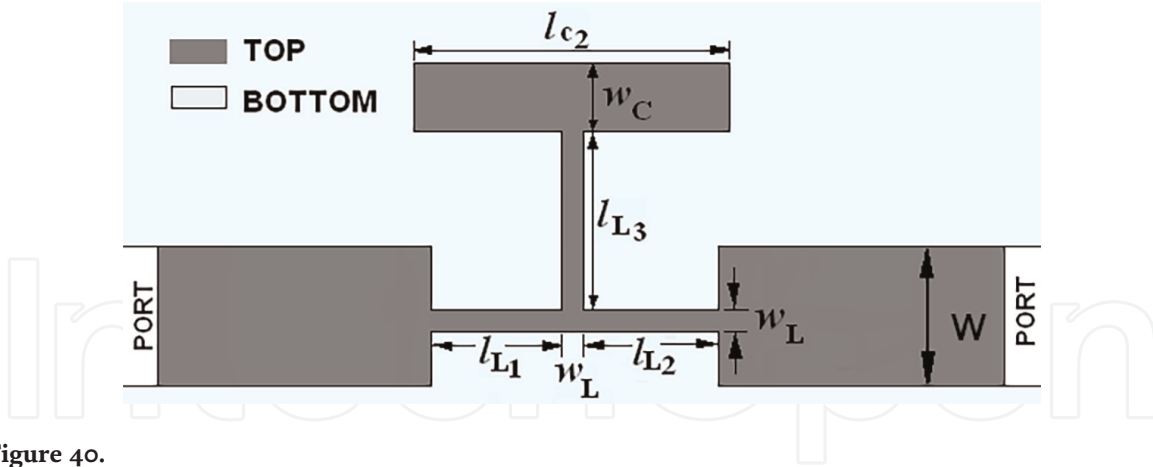


**Figure 40.** Schematic diagram of the lowpass filter using open-ended T-shaped stub.

$$l_{Li} = \frac{\lambda_{gL}(f_c)}{2\pi} \sin^{-1} \left( 2\pi f_c \frac{L_i}{Z_{0c}} \right) \quad (11)$$

$$l_{Ci} = \frac{\lambda_{gC}(f_c)}{2\pi} \sin^{-1} (2\pi f_c Z_{0c} C_i) \quad (12)$$

#### 2.4.2 Simulated result of the third order elliptic filter

The MoM based EM simulation verifies the design, and the simulated frequency response is illustrated in **Figure 41**. It is clear from the simulation that the upper stopband of the LPF is relatively poor, about 820 MHz at a  $-15$  dB attenuation level. The sharpness factor is 34.7 dB/GHz, with cutoff frequency and pole frequency being 3.3 GHz and 4.5 GHz, respectively.

#### 2.4.3 Bandwidth improvement by DGS units

This third-order elliptic function LPF is then modified by the four split ring-shaped DGS structures. The four DGS units are of different sizes and are distributed in two concentric sets. Each of these sets is constructed by a pair of split ring DGS units and placed on two sides of the LPF. This modified LPF layout is given in **Figure 42**. The dimension of the split ring DGS are:- the inner radius of the smaller split ring DGS placed at the left-hand side,  $r_1 = 3$  mm, the outer radius of the smaller split ring DGS placed at the left-hand side  $r_1' = 3.3$  mm, the inner radius of the bigger split ring

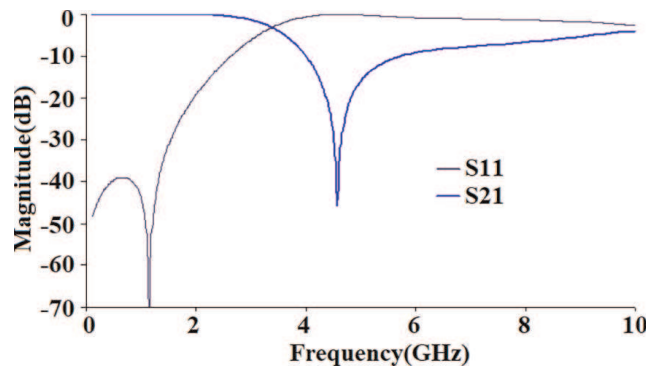


**Figure 41.** S-parameter response of the open-ended T-shaped stub.

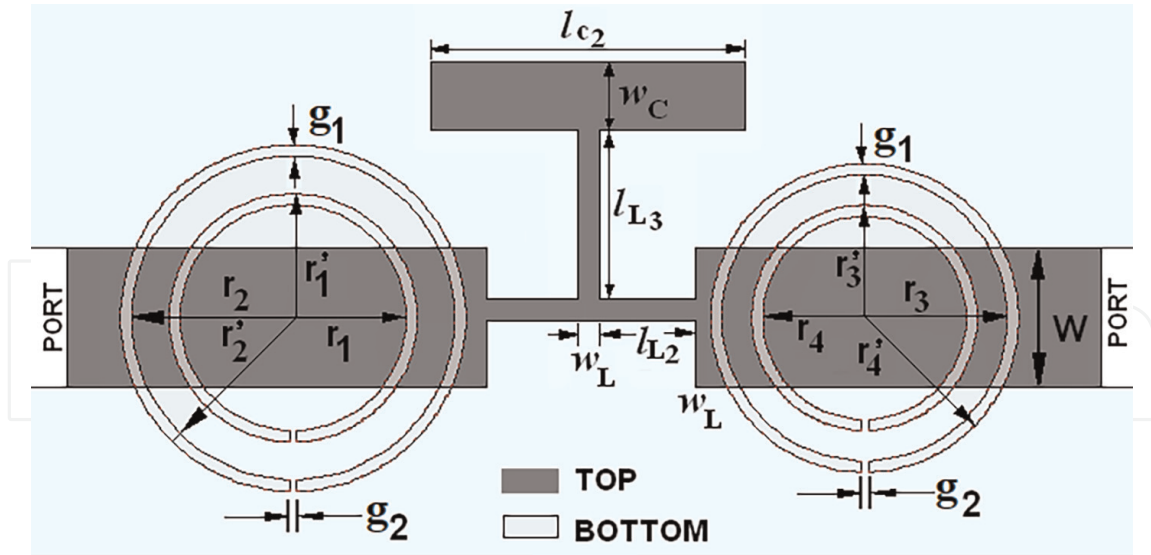


**Figure 42.**  
 Schematic diagram of the lowpass filter using open-ended split ring DGS sections and T-shaped stub.

DGS placed at the left-hand side  $r_2 = 4.3$  mm, the outer radius of the smaller split ring DGS placed at the left-hand side  $r_2' = 4.6$  mm, the inner radius of the smaller split ring DGS placed at the right-hand side  $r_3 = 2.7$  mm, the outer radius of the smaller split ring DGS placed at the right-hand side  $r_3' = 3$  mm, the inner radius of the bigger split ring DGS placed at the right-hand side  $r_4 = 3.7$  mm, the outer radius of the bigger split ring DGS placed at the right-hand side  $r_4' = 4.1$  mm, the distance between two sets of DGS units,  $L = 15$  mm, the slot widths of the four DGS units are same and are given by,  $g_1 = 0.3$  mm, the split gaps of the DGS units are also alike and are referred to as,  $g_2 = 0.2$  mm.

#### 2.4.4 Simulated result of the modified third order elliptic filter with DGSs

The design is simulated, and the corresponding simulated response is shown in **Figure 43**. It is evident from the response that the filter's stopband is increased, and  $-15$  dB bandwidth is obtained as  $2.7$  GHz. The proposed filter exhibit four transmission zeros responsible for four DGS units. These pole frequencies occur at  $3.1$  GHz,  $3.9$

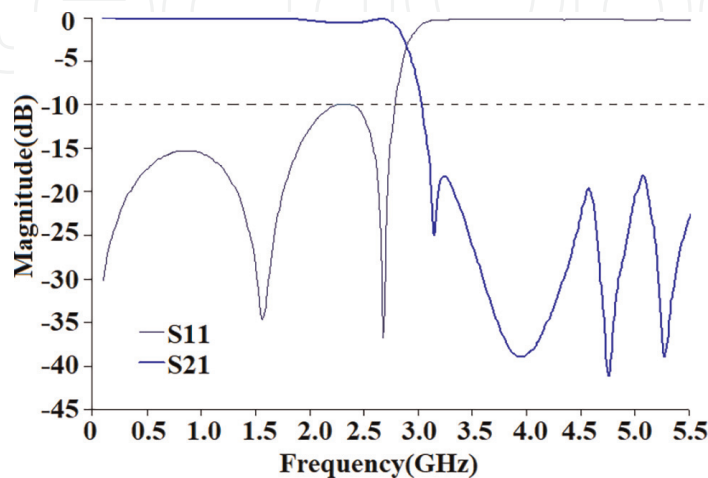


**Figure 43.**  
 S-parameter response of the lowpass filter using double unit split ring DGS sections and Open-ended T-shaped stub.



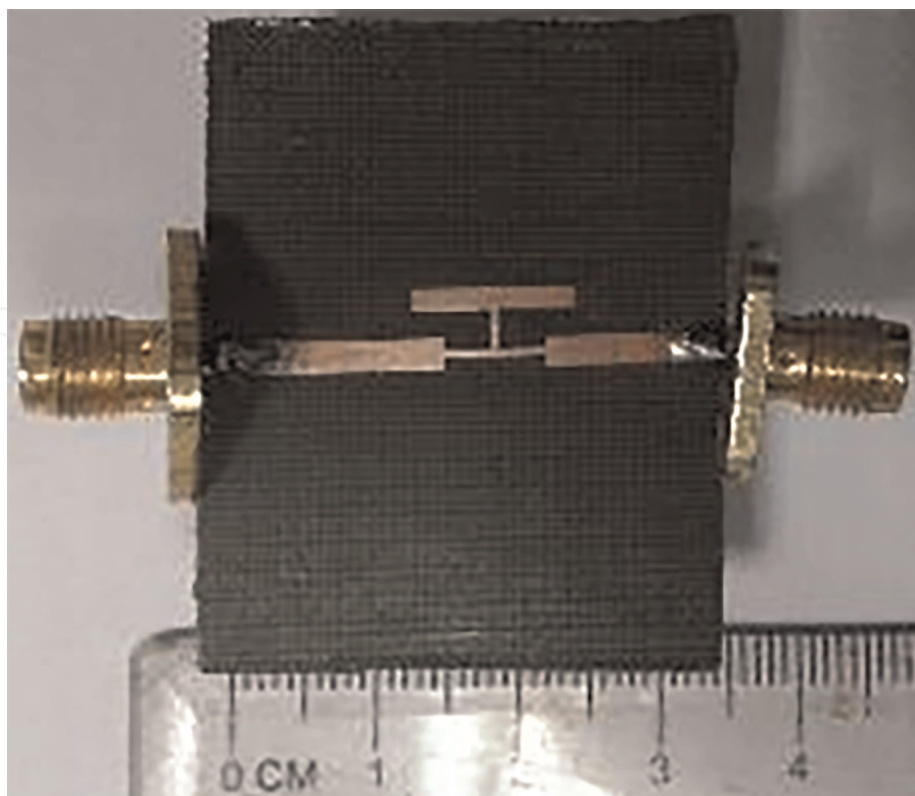


**Figure 44.**  
*Photographic view of the fabricated prototype top plane.*

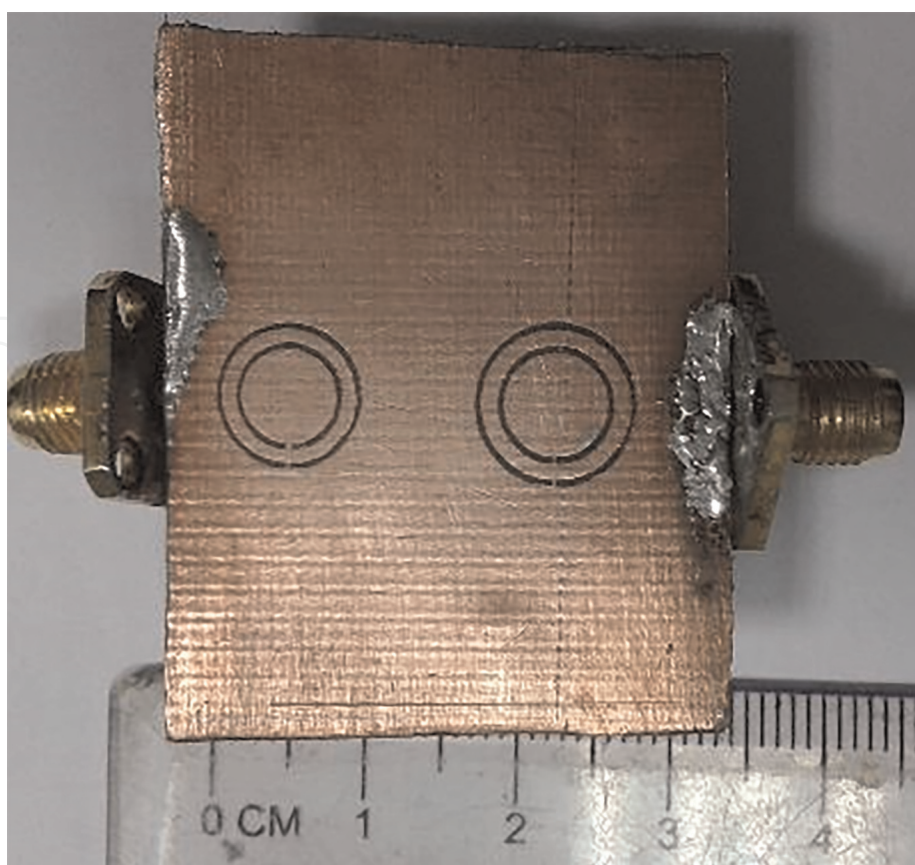


**Figure 45.**  
*Photographic view of the fabricated prototype bottom plane.*

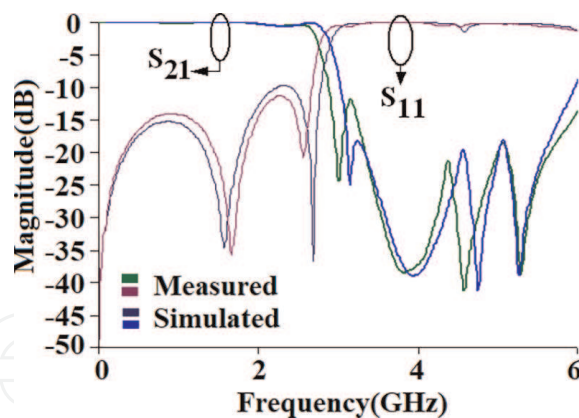


**Figure 46.**  
*Comparison of the simulated and measured S-parameter result.*

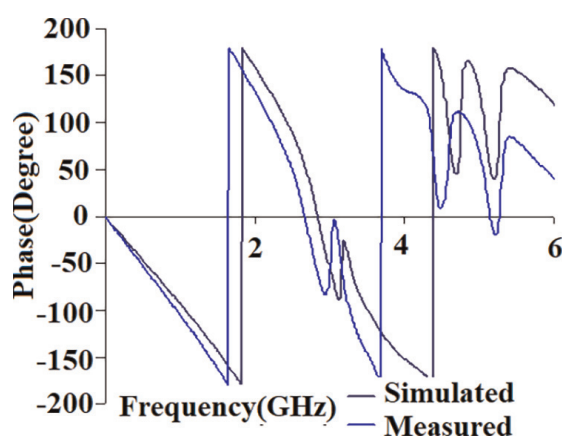


**Figure 47.**  
*Comparison of the simulated and measured phase response.*

GHz, 4.7 GHz, and 5.2 GHz. The filter's cutoff frequency is obtained at 2.89 GHz with an insertion loss of less than 0.5 dB. The maximum rejection level of the stop-band is 16.3 dB, and the sharpness factor is increased to 100.9 dB/GHz. Therefore the proposed filter provides greater bandwidth and sharper roll-off factor by applying the four split ring-shaped DGS units.

#### 2.4.5 Measured result of the modified third order elliptic filter with DGSs

The fabricated prototype verifies the simulated response, and a photograph of the fabricated layout is shown in **Figures 44** and **45**. There is good agreement between simulated and measured results, plotted in **Figures 46** and **47**, showing the variation of simulated and measured phase response with the frequency.

### 3. Conclusions

Here in this chapter, different DGS structures and their characteristics are studied. The hexagonal head dumbbell DGS provides stopband performance with a 4.3% reduced size than the conventional square head dumbbell DGS. The circular split ring DGS is very compact and provides a bandstop response. This type of structure has a very narrow slot gap and a very small cross-sectional area of  $0.07 \lambda_0 \times 0.07 \lambda_0$ . This

| References                      | Compactness<br>$\lambda_0 \times \lambda_0$   | Sharpness factor at lower side<br>(dB/GHz) | Insertion Loss at<br>passband (dB) |
|---------------------------------|---|--|------------------------------------|
| [4]                             | $0.13 \times 0.33$                            | 5.1  | —                                  |
| [17]                            | $0.30 \times 0.06$                            | 6  | —                                  |
| [5]                             | $0.03 \times 0.08$                            | 51.1                                       | -1.3                               |
| [9]                             | $0.07 \times 0.11$                            | 45   | -0.43                              |
| Proposed unit DGS<br>structures | Compactness $\lambda_0$<br>$\times \lambda_0$ | Sharpness factor at lower side<br>(dB/GHz) | Insertion Loss at<br>passband (dB) |
| Hexagonal shape                 | $0.04 \times 0.12$                            | 11.6                                       | -0.03                              |
| Circular Split ring<br>shape    | $0.07 \times 0.07$                            | 79.2                                       | -0.07                              |

**Table 9.**

*Some advantages of the proposed DGS structures as compared to state of the art.*


DGS structure also provides a very sharp roll-off factor of 79.2 dB/GHz. The above table (**Table 9**) provides some advantages of the proposed DGS structures compared to some unit structures available in the literature. Since here, the main intention is to compare the qualitative analysis of the proposed DGS units to that of the DGS units available in the literature. Due to the non-availability of data, some insertion loss boxes in the above table are kept blank.

## Author details

Somdotta Roy Choudhury  
Ramrao Adik Institute of Technology, D.Y. Patil Deemed to be University,  
Navi Mumbai, India

\*Address all correspondence to: somdottaroychoudhury@gmail.com

## IntechOpen

© 2022 The Author(s). Licensee IntechOpen. This chapter is distributed under the terms of the Creative Commons Attribution License (<http://creativecommons.org/licenses/by/3.0>), which permits unrestricted use, distribution, and reproduction in any medium, provided the original work is properly cited. 

## References

- [1] Radisic V, Qian Y, Coccioli R, Itoh T. Novel 2-D photonic bandgap structures for microstrip line. *IEEE Microwave Guided Wave Letters*. 1998;**8**:69-71. DOI: 10.1109/75.658644
- [2] Yang F-R, Ma K-P, Qian Y, Itoh T. A uniplanar compact photonic-band gap (UC-PBG) structure and its applications for microwave circuits. *IEEE Transactions on Microwave Theory and Techniques*. 1999;**47**:1509-1514. DOI: 10.1109/22.780402
- [3] Kim C-S, Park J-S, Ahn D, Lim J-B. A novel 1-D periodic defected ground structure for planar circuits. *IEEE Microwave Guided Wave Letters*. 2000;**10**:131-133. DOI: 10.1109/75.846922
- [4] Ahn D, Park J-S, Kim C-S, Kim J, Qian Y, Itoh T. A design of the low-pass filter using the novel microstrip defected ground structure. *IEEE Transactions on Microwave Theory and Techniques*. 2001;**49**:86-93. DOI: 10.1109/22.899965
- [5] Rahman A-B-A, Verma A-K, Boutejdar A, Omar A-S. Control of bandstop response of Hi-Lo microstrip low-pass filter using slot in ground plane. *IEEE Transactions on Microwave Theory and Techniques*. 2004;**52**:1008-1013. DOI: 10.1109/TMTT.2004.823587
- [6] Man M-K, Sanyal S. A novel defected ground structure for planar circuits. *Microwave & Wireless Component Letters*. 2006;**16**:93-95. DOI: 10.1109/LMWC.2005.863192
- [7] Karmakar N-C, Roy S-M. Quasi-static modelling of defected structure. *IEEE Transactions on Microwave Theory and Techniques*. 2006;**54**:2160-2168
- [8] Weng L-H, Guo Y-C, Shi X-W, Chen X-Q. An overview on defected ground structure. *Progress in Electromagnetics Research B*. 2008;**7**:173-189. DOI: 10.2528/PIERB08031401
- [9] Huang S-Y, Lee Y-H. A compact E-shaped patterned ground structure and its applications to tunable bandstop resonator. *IEEE Transactions on Microwave Theory and Techniques*. 2009;**57**:657-666. DOI: 10.1109/TMTT.2009.2013313
- [10] Parui S-K, Das S. Modeling of modified split-ring type defected ground structure and its application as bandstop filter. *Radio Engineering*. 2009;**18**:149-154
- [11] Biswas R-N, Kar A. A novel PSO-IE3D based design and optimization of a low profile Dual Slot Microstrip Patch Antenna. *IEEE Region 10 International Conference TENCON (TENCON '08)*; 19-21 November 2008; Hyderabad, India; 2009. p. 1-4
- [12] Pozar D-M. *Microwave Engineering*. 4th ed. USA: John Wiley & Sons; 2017. p. 399
- [13] Meyers R-G, Ye Q. Incorporation of Zeland's IE3D in the microwave and RF classroom. In: *IEEE Antennas and Propagation Society International Symposium (APS '02)*. San Antonio, TX; 2002. pp. 688-691
- [14] Park J-S, Kim J-H, Lee J-H. A novel equivalent circuit and modeling method for defected ground structure and its application to optimization of a DGS lowpass filter. *IEEE MTT-S International Microwave Symposium Digest*. 2002;**1**:417-420. DOI: 10.1109/MWSYM.2002.1011644

[15] Park J-S, Yun J-S, Ahn D. A design of the novel coupled-line bandpass filter using defected ground structure with wide stopband performance. *IEEE Transactions on Microwave Theory and Techniques*. 2002;**50**:2037-2043. DOI: 10.1109/TMTT.2002.802313

[16] Lim J-S, Kim C-S, Lee Y-T, Ahn D, Nam S. Design of lowpass filters using defected ground structure and compensated microstrip line. *Electronics Letters*. 2002;**38**:1357-1358. DOI: 10.1049/el:20020889

[17] Kim C-S, Lim J-S, Nam S, Kang K-Y, Ahn D. Equivalent circuit modelling of spiral defected ground structure for microstrip line. *Electronics Letters*. 2002;**38**:1109-1110. DOI: 10.1049/el:20020742